ME525 Applied Acoustics Lecture 26, Winter 2022
Mode interference and the 2 by 2 covariance matrix

Peter H. Dahl, University of Washington

This week some additional an important features of waveguide propagation will be discussed briefly followed by a discussion of studies in vector acoustics.

2-Mode interference

The interference pattern in range ΔR for a narrow band (e.g., $e^{\pm i\omega t}$) acoustic field depends on the differences of the horizontal wavenumbers Δk_{rn} of the various modes involved as in $\Delta R = \frac{2\pi}{\Delta k_{rn}}$. A multi-mode interference pattern will be difficult to interpret, however A 2-mode interference pattern is very distinctive. An example (Fig. 1) shows field oscillating at ranges greater than about 3 km, every 550 m. At this range there exists two remaining modes, modes 1 and 2, a few higher order modes existed near the source but have now decayed away owing to their higher attenuation.

In the example shown for a Pekeris waveguide $k_{r1} = 0.1675$ and $k_{r2} = 0.1561$ Put Δk_r as the difference, then $\frac{2\pi}{\Delta k_r}$ gives the precise "wavelength" of this interface pattern, which is about 550 m.

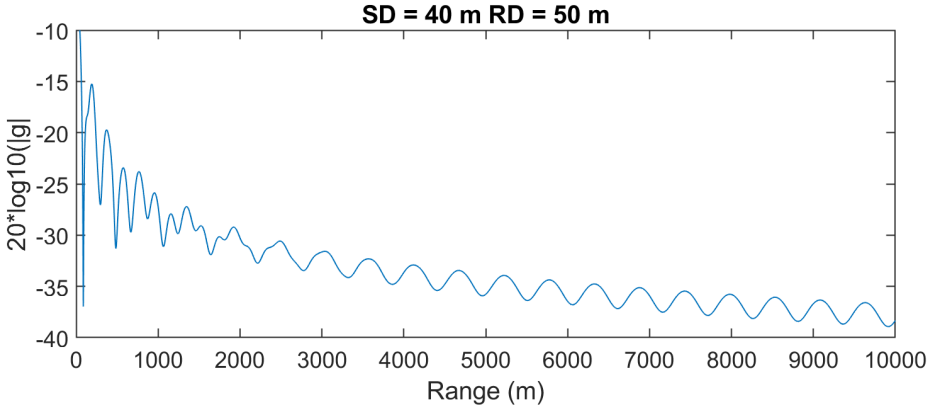

Figure 1: The field $20\log_{10}|g|$ for waveguide defined by depth 75 m, c_w 1470 m/s, c_b = 1800 m/s, frequency = 40 Hz. Higher order modes decay with range leaving only modes 1 and 2, where $k_{r1} = 0.1675$ m^{-1} and $k_{r2} = 0.1561$ m^{-1}. The 2-mode interference pattern repeats every $\frac{2\pi}{\Delta k_r}$ m, or about 550 m.

Eigenvalues and eigenvectors of 2 by 2 Covariance Matrix

Much of this segment is discussed on the board. Figure 2 shows the eigenvectors for the matrix A that multiplies a range of candidate vectors $\vec{b}$. Two eigenvectors will be such that $A\vec{x} = \lambda\vec{x}$, where

λ is an eigenvalue. In one case (left) the matrix A is given by

$$A = \begin{pmatrix} 3 & 2 \\ 0.5 & 2.5 \end{pmatrix} \tag{1}$$

In other case (right) the matrix A is given by and is symmetric matrix.

$$A = \begin{pmatrix} 3 & 2 \\ 2 & 2.5 \end{pmatrix} \tag{2}$$

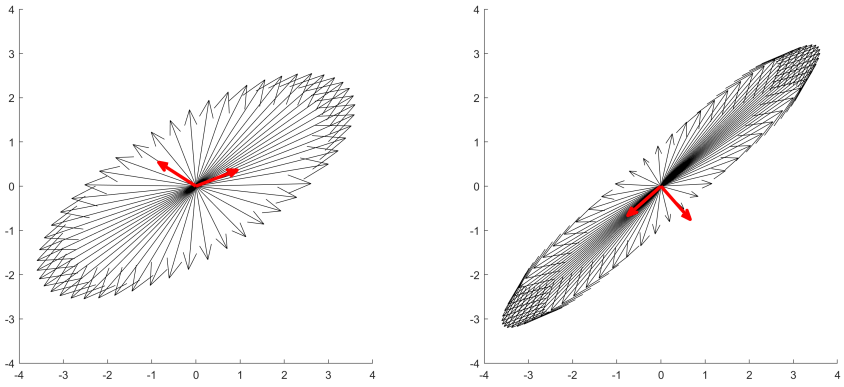

Figure 2: Left: The many set of vectors formed by $\vec{x} = A\vec{b}$ for matrix A, two of which are eigenvectors (red) because they are parrallel to $\vec{b}$. Right: same situation but with matrix A being a symmetric matrix yield two eigenvectors that are orthogonal.

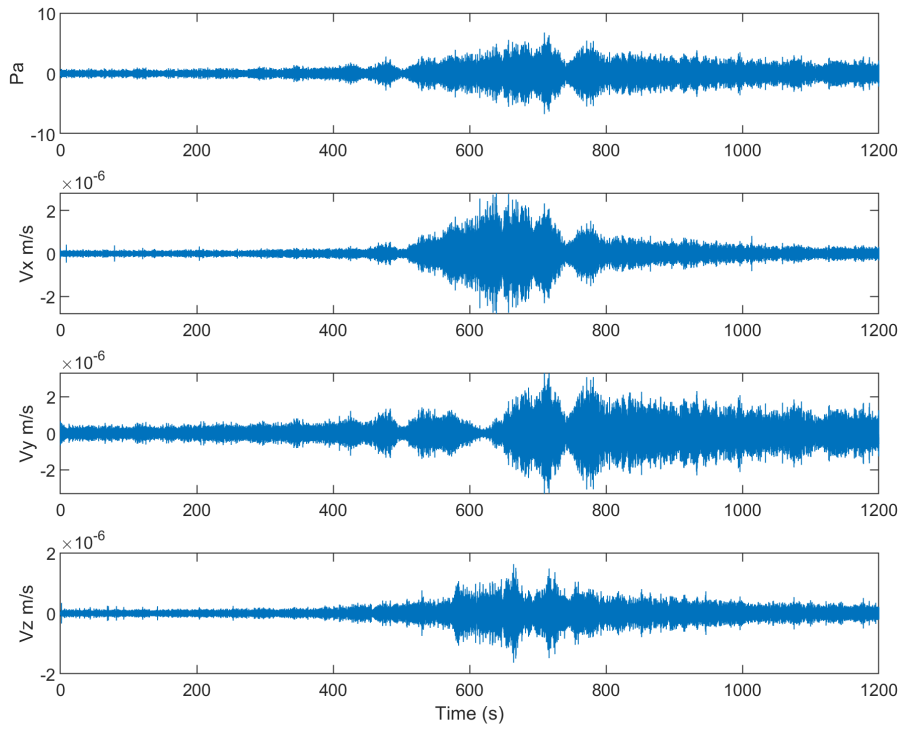

Figure 3: Acoustic pressure and velocity time series $V_{x,y,z}$ filtered withing a 63-Hz third octave band for the CPA of the *M/V Oregon Highway* passing by the IVAR system at CPA range $\sim$ 450 m.

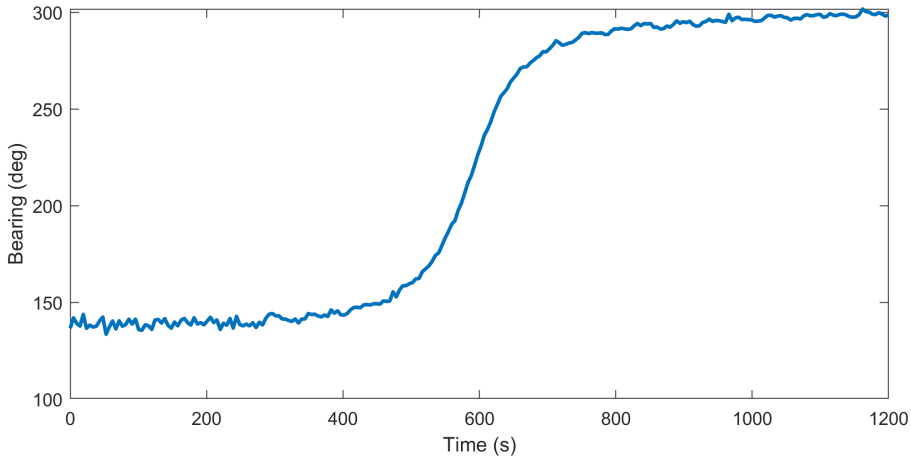

Figure 4: Bearing of the *M/V Oregon Highway* passing by the IVAR system estimated from the eigenvectors of the V_x, V_y covariance matrix

ME525 Applied Acoustics Lecture 27, Winter 2022
Mode group and phase velocity, the 3 by 3 covariance matrix

Peter H. Dahl, University of Washington

This week some additional an important features of waveguide propagation will be discussed briefly followed by a discussion of studies in vector acoustics.

Mode group and phase velocity

A very important property of underwater waveguide propagation of sound is the phenomenon of the speed of energy transport for a given mode, which depends on frequency. Since the modes depend on geometry, i.e., primarily water depth H, this is known as geometric dispersion (e.g. Frisk, 1994).

The easiest way to fathom this is to examine the propagation of a short pulse of sound (Fig. 1) consisting of many frequencies all intially transmitted at once-in other words the pulse is broadband, such as that from explosive source. See also Fig. 3 of Lecture 6 representing a pulse from an explosive source measured at range 5000 m. The result in (Fig. 1, upper) is a simulated time series for range 12000 m based on the similar conditions approximated by a Pekeris waveguide with water speed $c_w = 1468$m/s, sediment speed $c_b = 1830$ m/s and water depth $H = 74$ m.

Observe that the "main" pulse arrives after a delay of abou 8 s, consistent with nominal value of range divided by c_w. However prior to the main pulse there exists low-amplitude arrival which slowly grows in amplitude. This is the ground wave which has traveled at the faster speed in the sea bed. The pulse continues to evolve, with different frequency content arriving at different times. This is dispersion.

This evolution of time and frequency is seen in the corresponding time-frequency plot or spectrogram of the simulated time series (Fig. 1, lower). The display is not a perfect rendition,–there is always a trade-off in terms balancing necessary time and frequency resolution– but it clearly reflects a pattern of five segments, representing the *group velocity*, V_n of modes 1-5 for frequencies 5 to 100 Hz. Let's parse this out: mode 1 is the largest pattern and seems to start around 10 Hz. There appears to be no support in the spectrogram for frequencies less than about 10 Hz, so 10 Hz is the cut-off frequency for mode 1 and hence the waveguide. Run Eq.(2) of Lecture 25 with these numbers–looks like 10 Hz just make the cut–but 8 Hz too low. The next pattern is mode 2, which appears to be supported by frequencies greater than about 25 Hz–again, Eq.(2) will show that 25 Hz just makes the cut for supporting now two modes.

Imagine now turning the pattern in Fig. 1 (lower) 90° clockwise, so time is on the vertical axis, and 8 s represents a faster speed than 8.5 s and so on. For example 8 s corresponds to approximately 1400 m/s and 9 s to approximately 1300 m/s. We could say this new rotated figure represents the

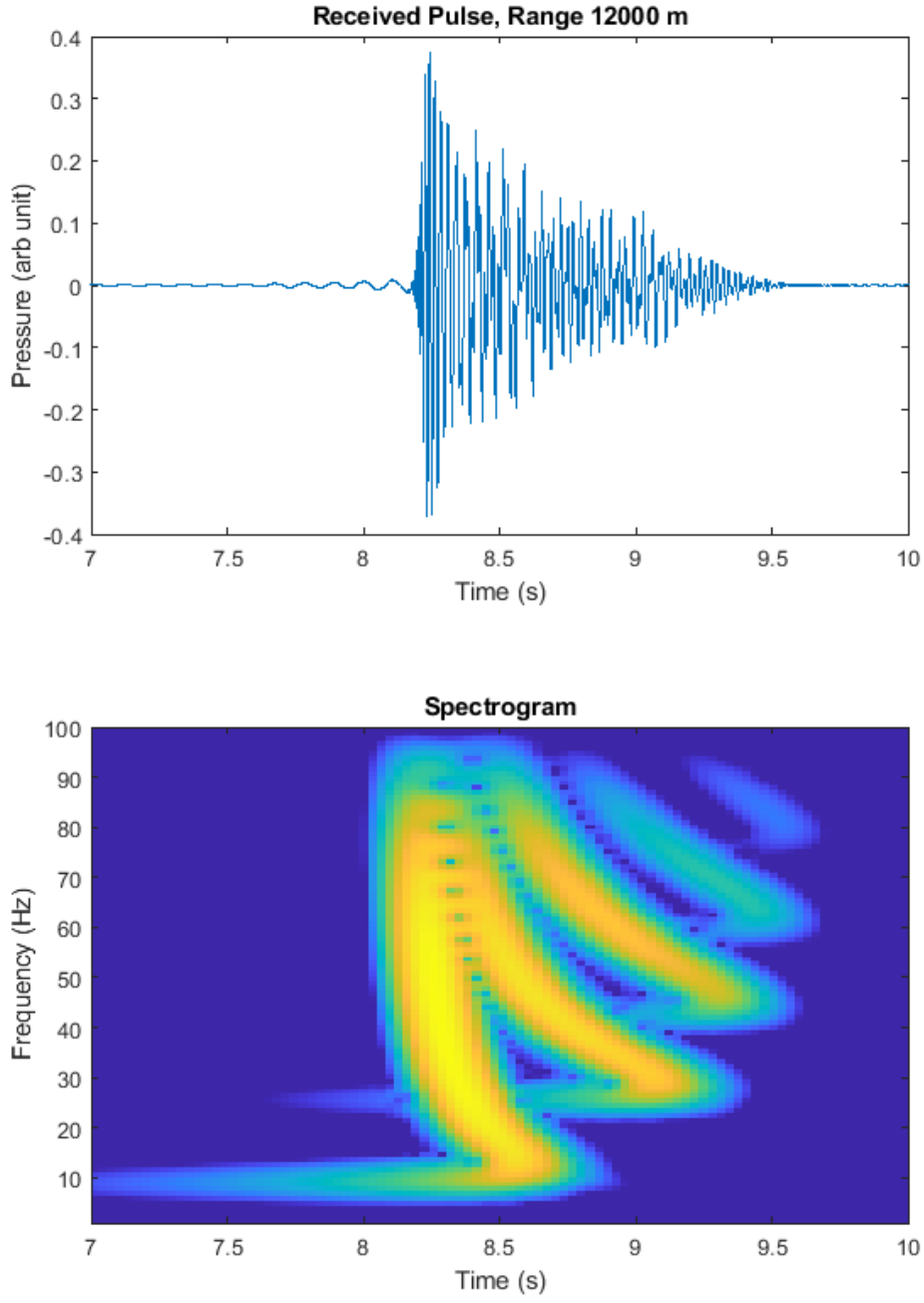

Figure 1: Upper: synthetic broad band pulse computed for received range of 12000 m for the Pekeris waveguide discussed in text. Lower: spectrogram of the received pulse showing 5 modes.

dispersion curves as function of frequency f for modes 1-5, or $V_n(f)$ n =1 to 5.

But what are they? One useful way to think about V_n is that for $n = 1$, or lowest order mode, the horizontal angle θ_n is also the lowest possible, so consequently there are the fewest reflections

between the sea surface and seabed as function of range (up and down cycles), thus the V_n is generally higher for mode 1. As n increases there are more up/down cycles (reflections) and one can intuit that it takes a bit more time for the acoustic energy to travel down the waveguide. It is somewhat more complicated than that, but this is useful starting interpretation.

The exact set of dispersion curves for this case through modes 1-4 are shown in Fig. 2. Now rotate this figure 90° counter-clockwise and observe the similarities between it and my spectrogram in Fig. 1. Note this figure also includes the phase velocities C_n–these are simple to compute: given the horizontal wavnumber for each mode k_{rn}, then $C_n = \frac{\omega}{k_{rn}}$. The very interesting minimum in

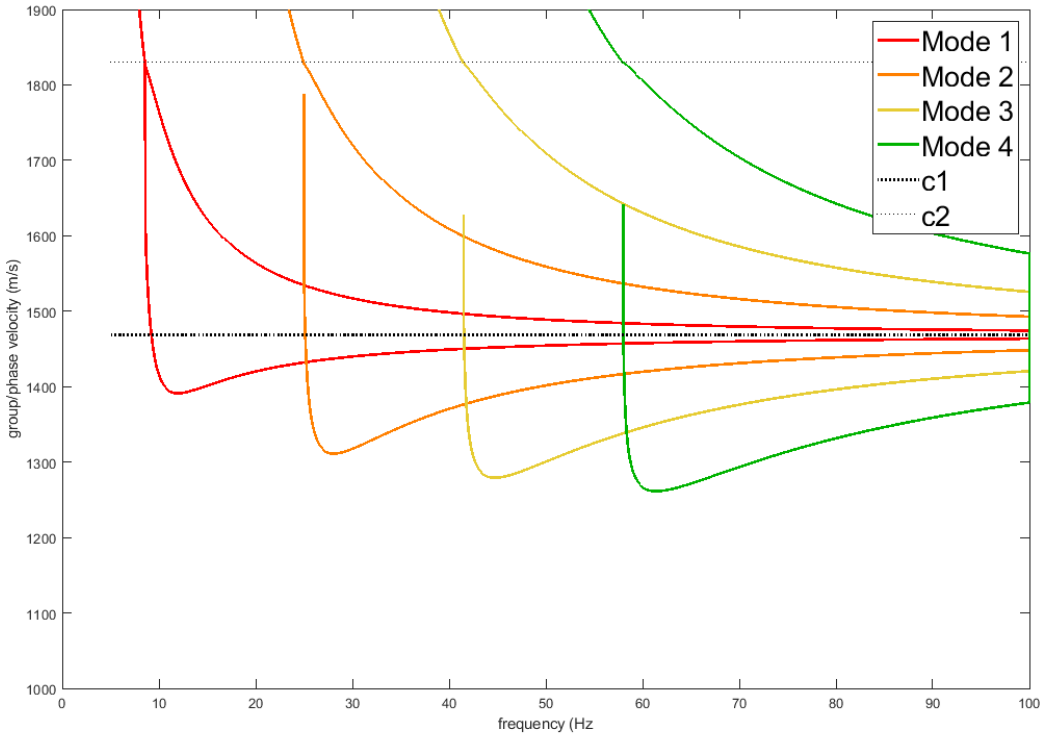

Figure 2: The group $V_n(f)$ and phase $C_n(f)$ velocities as a function of frequencies for the Pekeris waveguide discussed in text.

$V_n(f)$ for each mode is known as the Airy phase. It can be observed in real data representing the reception of an initially broad pulse, such as from an explosive source or air gun used in geophysical exploration, after that pulse has traveled a sufficient range for dispersion to be observed. Look closely at my time-series simulation in Fig. 1 around time 8.5 s and 9 s, where the frequency appears to be somewhat lower. These regions likely correspond to the Airy phase contribution from modes 1 and 2, respectively.

The standard way many of us learned to compute V_n is through the following formal definition:

$$V_n = \frac{d\omega}{dk_{rn}} \tag{1}$$

where you will recall that k_{rn} is the horizontal wavenumber for the n^{th} mode. This can be quite delicate to compute numerically–typically one needs to evaluate modes over a fine frequency spacing, take the finite difference and hope it works. For the Pekeris waveguide involving just two media water and sediment, each with separate sound speeds and densities, Frisk (1994, pp. 152-154) also provides a handy analytical formulas, with results for the case under discussion shown in Fig. 2.

An alternative way (Chapman and Ellis, 1983) that I find easy to implement is

$$V_n = \frac{\int_0^\infty U_n^2(z)/\rho(z)dz}{C_n \int_0^\infty U_n^2(z)/(\rho(z)c(z)^2)dz} \tag{2}$$

where $U_n(z)$ is the unique normal mode function at a given frequency. Thus, for the cases we have been discussing, e.g., see Eqs. (3) and (5) of Lecture 25, $U_n(z) = \sin(\gamma_n z)$. Check the dimension of Eq.(2)–does it make sense? Some care is still needed to evaluate Eq.(2). For example, the behavior of the normal mode function for a more realistic Pekeris waveguide changes from $\sin(\gamma_n z)$ to decaying exponential for $z > H$ (see Fig. 4 of Lecture 25). As a test, though, let us use the case of the rigid boundary condition on the seabed, e.g., as in Eq. (3) of Lecture 25. In this case the integral in Eq.(2) is limited to between 0 and water depth H. The result (Fig. 3) for case of $H = 20$ m, and water sound speed of 1525 m/s for the first four modes shows that the cut-off frequency for this waveguide is about 19 Hz. Notice that V_n for this rigid boundary case are quite different from the Pekeris case in Fig. 2, with the notable absence of an Airy phase.

The phase velocities, however, are somewhat more realistic. Indeed this property is often exploited in a technique known as "warping" (Fig. 4), which takes a spectrogram from a received broadband signal and "warping" it, or straightening it, to follow the phase velocities of an "equivalent" rigid boundary waveguide. For example, the thin red lines in the lower right panel of Fig. 4 shows such phase velocities.

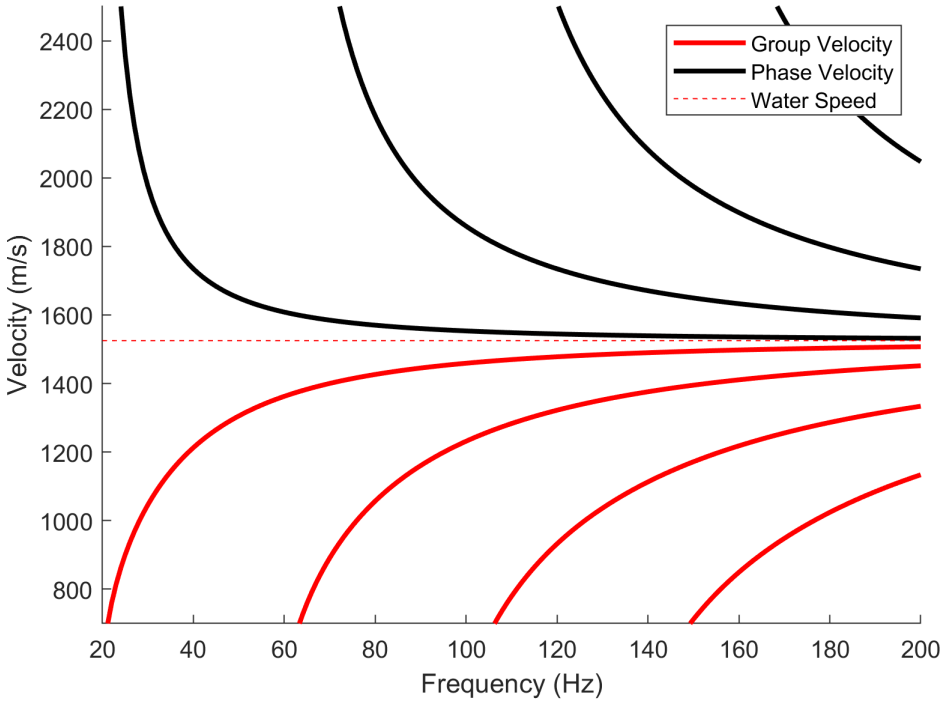

Figure 3: The group $V_n(f)$ and phase $C_n(f)$ velocities as a function of frequencies for waveguide of depth H 20 m, water speed 1525 m/s, and rigid boundary condition for water-seabed interface.

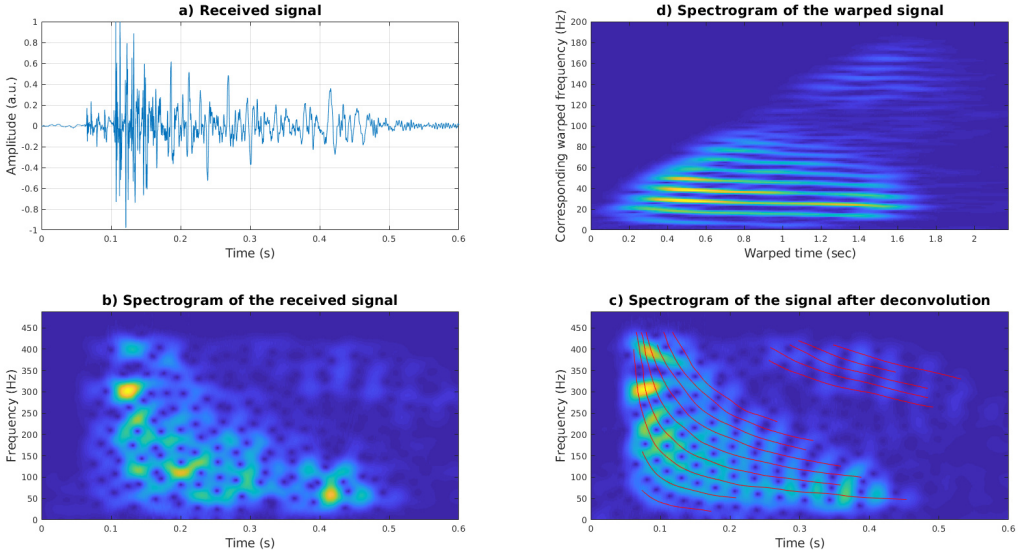

Figure 4: Figure supplied by my colleague Julien Bonnel, of Woods Hole Oceanographic Institution. See also Bonnel and Chapman, 2011.

Eigenvalues and eigenvectors of 3 by 3 Covariance Matrix

We continue with the 63-Hz third octave measurements of the ship Oregon Highway started last time. Now take the three velocity sensors from the IVAR system, V_x, V_y, V_z and construct the 3 by 3 covariance matrix $S3$ as follows:

$$S3 = \begin{pmatrix} \langle V_x^2 \rangle & \langle V_x V_y \rangle & \langle V_x V_z \rangle \\ \langle V_y V_x \rangle & \langle V_y^2 \rangle & \langle V_y V_z \rangle \\ \langle V_z V_x \rangle & \langle V_z V_y \rangle & \langle V_z^2 \rangle \end{pmatrix} \tag{3}$$

where the angle brackets as in $\langle V_x^2 \rangle$ represent a 5-s average over the data shown in Fig. 3 of Lecture 26.

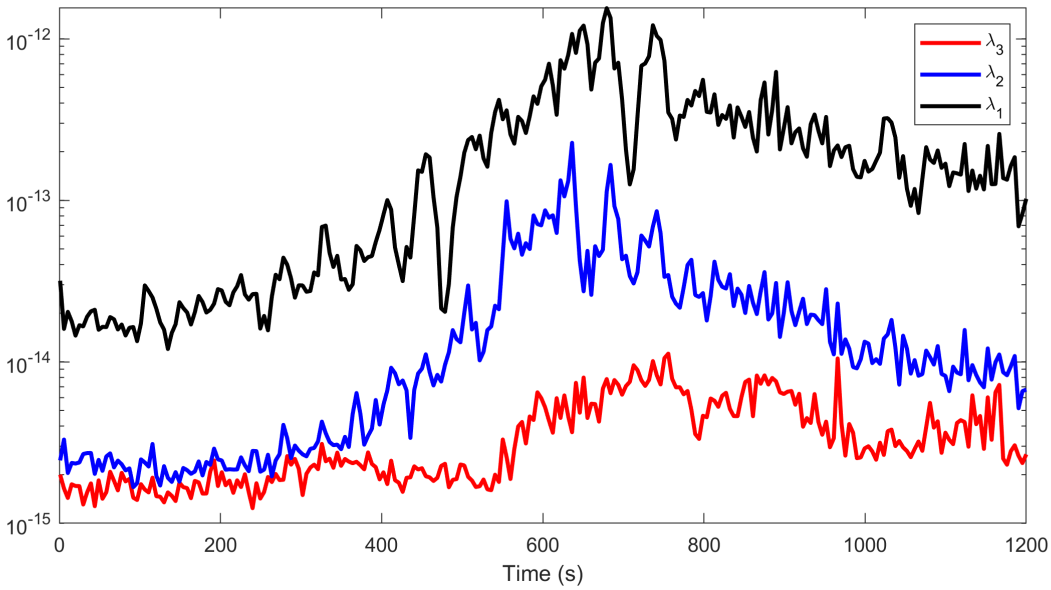

Figure 5: The three eigenvalue over time (based on 5 sec avg) for the CPA of the Oregon Highway

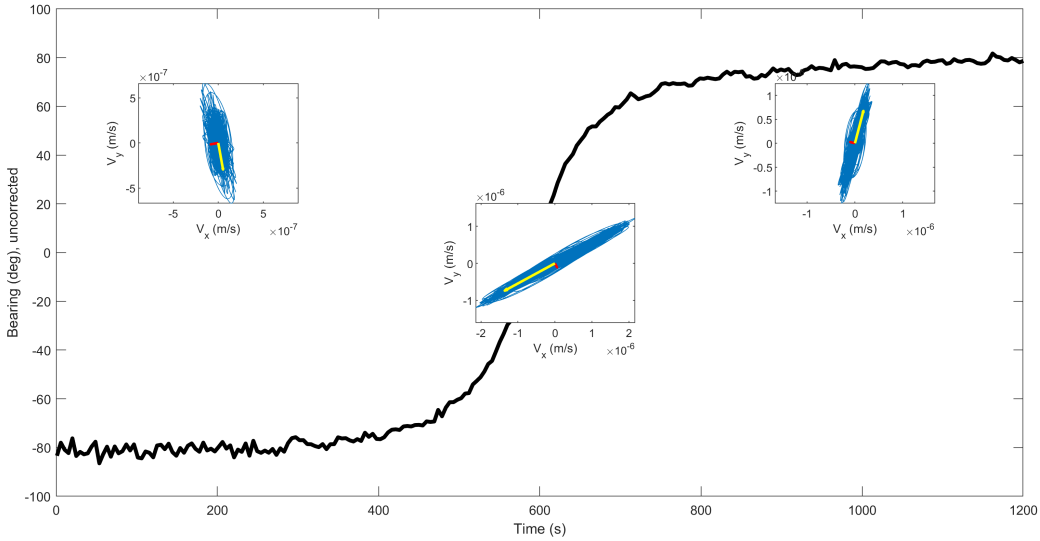

Figure 6: Bearing of the Oregon Highway (not corrected for IVAR orientation) showing three cases of $V_x(t), V_y(t)$ and the principal axes obtained by the eigenvectors. The yellow defines the bearing (uncorrected).

References

Frisk, G. V. *Ocean and Seabed Acoustics* (Prentice Hall, Englewood Cliffs, NJ, 1994)
D. M. F. Chapman, and D.D. Ellis, "The group velocity of normal modes," *J. Acoust. Soc. Am.* 78, 983-979, 1983
J. Bonnel and N. R. Chapman, "Geoacoustic inversion in a dispersive waveguide using warping operators" *J. Acoust. Soc. Am.* EL101, 2011

ME525 Applied Acoustics Lecture 28, Winter 2022
The depth-dependent Green's function; the 4 by 4 field matrix

Peter H. Dahl, University of Washington

This week some additional an important features of waveguide propagation will be discussed briefly followed by a discussion of studies in vector acoustics.

The depth-dependent Green's function for a Pekeris waveguide

The following is the most brief of introductions–perhaps too brief–but meant to give additional perspective on the Green's function for an underwater waveguide with cylindrical symmetry, as summarized by the modal summations formulas in Lecture 25; these in the form of Eq. (3), representing rigid (infinite impedance) boundary condition on the seabed and Eq.(5) representing finite impedance condition separating water and seabed halfspace, or the Pekeris waveguide. The perspective originates from examining these functions with a completely equivalent representation based on the Hankel transform of a depth-dependent Green's function (Frisk, 1994).

The depth-dependent Green's function for the Pekeris case (Frisk, 1994, Eq. 6.64) is

$$g(k_r) = \frac{i(e^{i\gamma|z-z_s|} - e^{i\gamma(z+z_s)} + Re^{2i\gamma H}(e^{-i\gamma(z+z_s)} - e^{-i\gamma|z-z_s|}))}{\gamma(1+Re^{2i\gamma H})}. \tag{1}$$

Things to notice: (i) the variable range r is missing, (ii) there remains the depth variable z, and constant for source depth z_s, (iii) the mode horizontal wave number k_{rn} and vertical γ_n are missing the indices n and appear to assume continueous distribution of values, and, importantly, (iv) the denominator should look familiar where R is the reflection coefficient of the seabed.

The field, for example, as in the discrete modal sum version given in Eq. (5) of Lecture 25, is recovered via a Hankel transform of $g(k_r)$ over the continuous distribution of horizontal wavenumbers k_r, yielding

$$g(r,z,z_s) = \int_0^\infty g(k_r)J_0(k_r r)dk_r \tag{2}$$

where J_0 is the 0^{th} order Bessel function. How to think of this? The Hankel transform is transforming from wavenumber domain, k_r, to a spatial domain in terms of range r, akin to Fourier transform with time and frequency.

As an example take the Pekeris waveguide (Fig. 1) with water speed $c_w = 1450$m/s, sediment speed $c_b = 1600$ m/s and water depth $H = 20$ m. Pick a frequency, say 220 Hz, and this waveguide looks to support about 3 trapped modes according to Eq.(2) of Lecture 25.

The Hankel transform must undertake a contour integral in the complex k_r-plane (Fig. 2) where a discrete set of poles, or singularities, each yield a residue contribution giving back the same

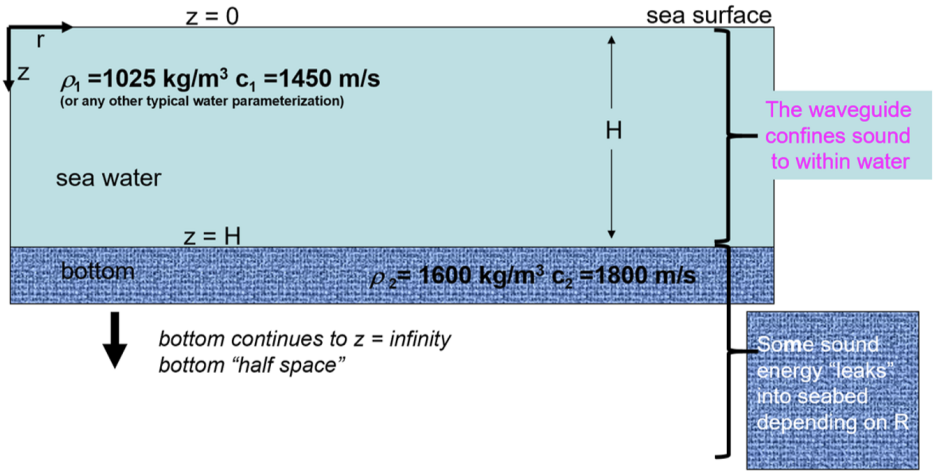

Figure 1: Pekeris waveguide. At a frequency of 220 Hz, this waveguide supports about three trapped modes.

solution we discussed previously involving a mode sum. The poles are located at discrete locations k_{rn}, with the figure depicting three such poles.

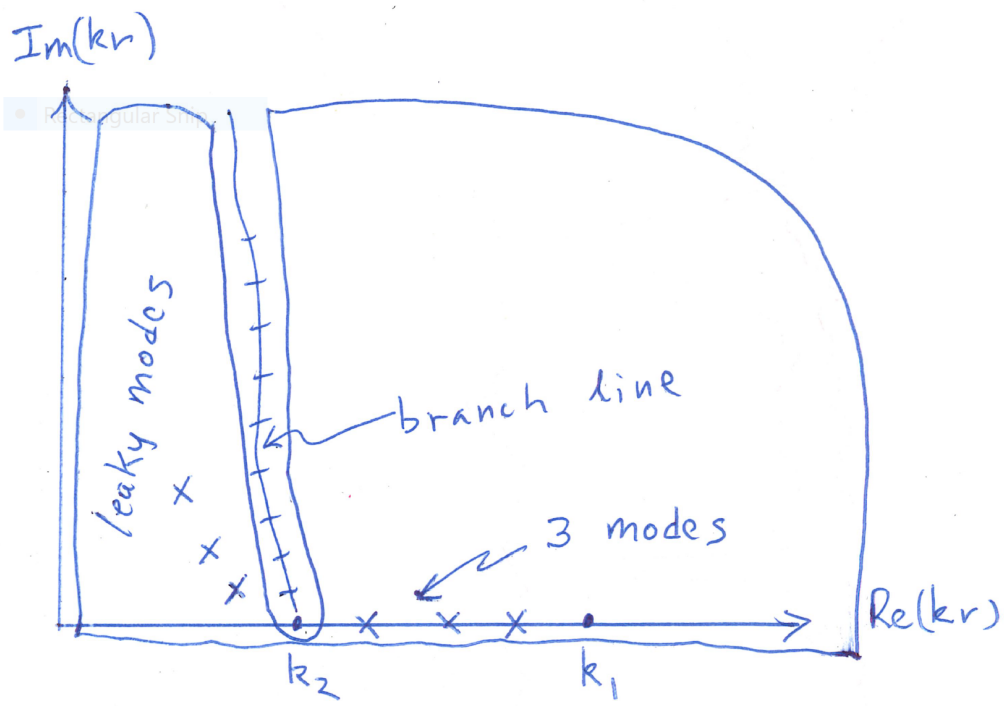

Figure 2: Sketch of the location of three trapped modes $k_{rn} n = 1, 2, 3$ located on the real-kr axis between wavenumbers k_1 (water layer) and k_2 seabed. A branch point is located at k_2, and to further to the left are a few leaky modes described by increasing imaginary part of the modal wavenumber. An integration contour is shown within which poles are located.

At the point on the complex k_r-plane located at k_2 there exists a *branch point* singularity. Here a choice must be made given the square-root ambiguity for $k_r = \pm k_2$. We choose $+k_2$ in accordance

with our convention of $e^{-i\omega t}$ and this prevents the integral from being unbounded and becoming infinite. But this choice necessitates a branch line integral along the contour shown in the figure. Notice: the branch point corresponds to the critical angle.

There are approximate, asymptotic solutions to the branch line integral (Frisk, 1994), otherwise numerical approaches are needed. Often the contribution of branch line integral is just ignored–just as it has in the solutions we've been discussing thus far consisting of a discrete modal summation. Why? Because it represents the continuum of angles $\theta > \theta_c$, as in Fig. 2 of Lecture 25, where such "equivalent" rays undergo significant reduction in amplitude upon each interaction with the seabed causing rapid attenuation with increasing range from the source.

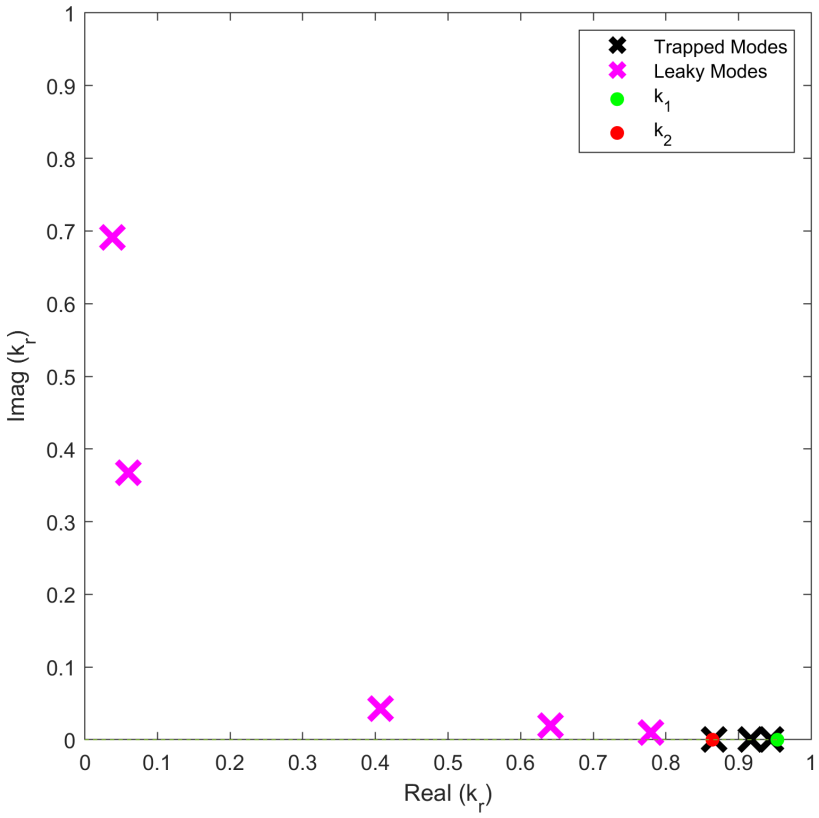

Figure 3: Situation in the complex k_r plane for the Pekeris waveguide of Fig. 1, when the frequency is 220 Hz. The waveguide supports about three trapped modes that are located between k_1 and k_2. Some leaky modes exist, with increasing imaginary component.

One clever way to deal with this branch line contribution to the integral is to recast the branch line singularity into a set of modes with increasing imaginary component, known as "leaky modes" as they leak energy into the seabed and rapidly attenuate. One of my favorite approaches is that of Zang and Tindle (1993) who capture this effect in their mode-finding algorithm, and these modes can thus included in a modal summation. They are referred to as "imperfect resonances" or "im-

proper modes" (Frisk, 1994); incontrast, one should think of a trapped mode as a complete or perfect resonance of the waveguide. A map of complex k_r plane (Fig. 3) shows the three trapped and four leaky modes along with their relation to the wavenumbers k_1 and k_2. There are many more leaky modes than the four shown–but the fourth one is a goner anyway, given its huge imaginary component, and probably only the first two leaky modes to the left of the branch point at k_2 make any meaningful contribution.

Figure 4 shows results of a computation involving both trapped plus leaky modes for the waveguide in Fig. 1, with frequency 220 Hz. It looks like by about range 50 m, the situation is fully described by the three trapped modes. Looking back to Fig. 2 from Lecture 25, I gave a range scale $R_o \approx \frac{H}{2\tan\theta_c}$ for the range delineating the transition from continuous + discrete modes to just discrete, or trapped, modes. You can confirm that R_o =21.4 m. Ok, maybe my R_o was a bit too conservative, and you might consider doubling it.

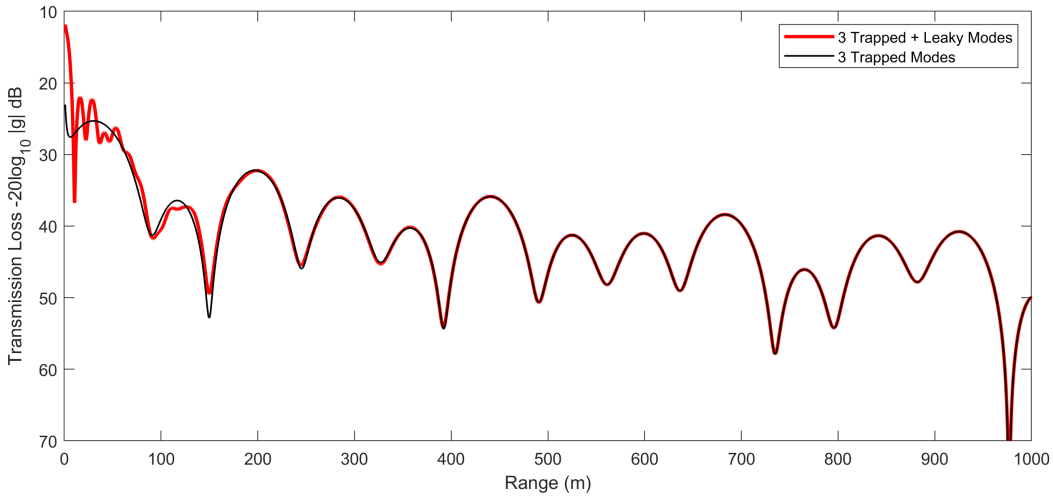

Figure 4: Pekeris waveguide. At a frequency of 220 Hz, this waveguide supports about three trapped modes.

The 4 by 4 Field Matrix

Thus far we've discussed 2 by 2 (V_x, V_y) and 3 by 3 (V_x, V_y, V_z) matrices based on vector acoustic measurements from the IVAR system. We were quite happy with pin-pointing the bearing of the ship *Oregon Highway*, based on a single time series of 63-Hz third octave narrow filtered data. The range of bearing angles over the observation period was about 160°. What would happen if the *Oregon Highway* did a circle around the IVAR system and the range was 360°? Now the rubber hits the road, and the full power of the IVAR system comes into play.

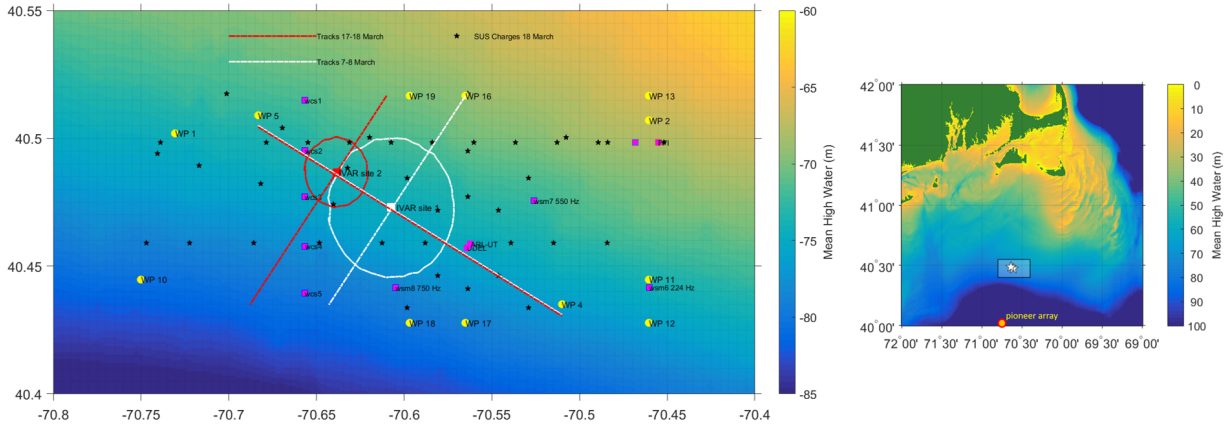

Figure 5: Track of the R/V Endeavor about the IVAR location (red circle) following circle at range 1.5 km, speed approximately 3 knots. Map on right shows the general location of the experiment which took place in March 2017.

Combine the pressure and velocity channels of the 4-channel IVAR system into a 4 by 4, what we refer to as a *field matrix* as follows:

$$F4 = \begin{pmatrix} \langle P^2 \rangle / z_0^2 & \langle PV_x \rangle & \langle PV_y \rangle & \langle PV_z \rangle \\ \langle PV_x \rangle & \langle V_x^2 \rangle z_0^2 & \langle V_x V_y \rangle z_0^2 & \langle V_x V_z \rangle z_0^2 \\ \langle PV_y \rangle & \langle V_y V_x \rangle z_0^2 & \langle V_y^2 \rangle z_0^2 & \langle V_y V_x \rangle z_0^2 \\ \langle PV_z \rangle & \langle V_z V_x \rangle z_0^2 & \langle V_z V_y \rangle z_0^2 & \langle V_z^2 \rangle z_0^2 \end{pmatrix} \tag{3}$$

where $z_0 = \sqrt{\rho c}$.

The matrix $F4$ is again symmetric, and will possess four real eigenvalues and four orthonormal eigenvectors, from which the bearing (Fig. 6) is unambiguously determined over a range of 360°. This bearing cannot be resolved in the same manner using only acoustic velocities V_x, V_y. The total energy, is equal to the trace of $F4$ divided by sound speed c, and the potential energy, equal to $F4(1,1)/c$ (Fig. 7). The potential energy is about 3 dB less than the total energy, indicating the remaining kinetic energy portion is approximately equal.

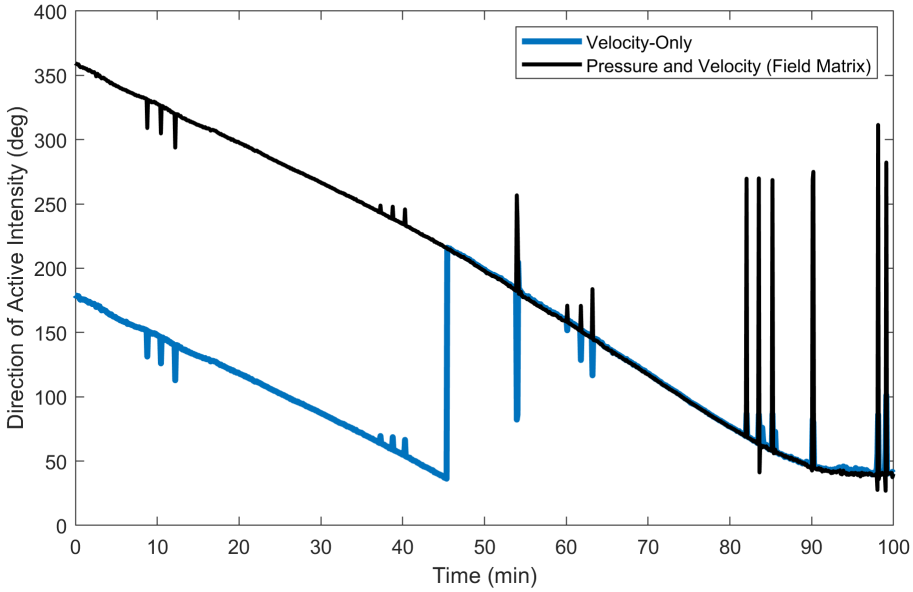

Figure 6: The bearing of sound radiating from the R/V Endeavor over the 260-305 Hz band, based on 4 by 4 (Acoustic Pressure + Velocity) and 3 by 3 (Acoustic Velocity only) observations. Abrupt changes are do to ongoing experiments involving small explosive sound sources.

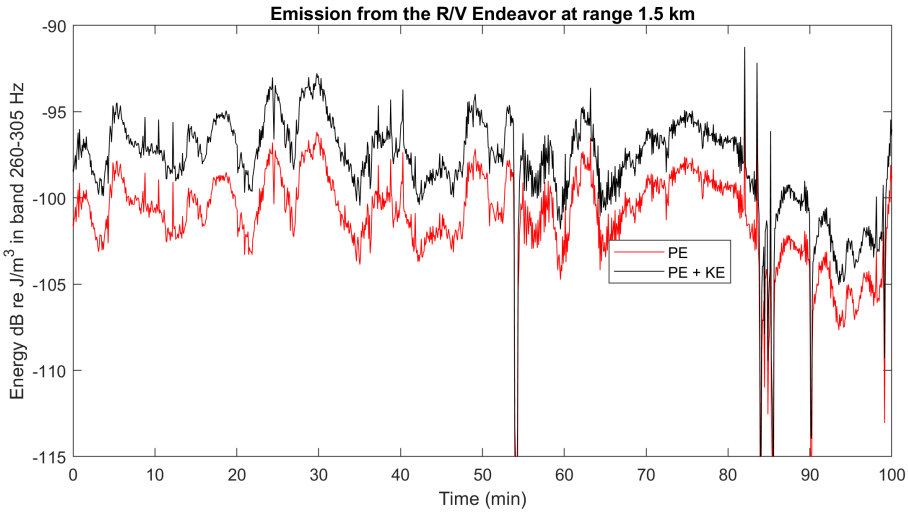

Figure 7: The total energy, and potential energy density (about 3 dB less) representing sound radiation from the R/V Endeavor while transiting in a circle about IVAR at range 1.5 km. Abrupt changes are do to ongoing experiments involving small explosive sound sources.

References

Frisk, G. V. *Ocean and Seabed Acoustics* (Prentice Hall, Englewood Cliffs, NJ, 1994)

Z. Y. Zang, and C. Tindle, "Complex effective depth of the ocean bottom" *J. Acoust. Soc. Am.* 93,205-213, 1993